

Electronic structure and spin polarization of $\text{Fe}_{1-x}\text{Mn}(\text{Co},\text{Ni})_x\text{S}_2$ alloys from first principles

Abdesalem Houari^{1,*} and Peter E. Blöchl²

¹ *Theoretical Physics Laboratory, Department of Physics, University of Bejaia, Bejaia, Algeria*

² *Clausthal University of Technology, Institute for Theoretical Physics,
Leibnizstr.10, D-38678 Clausthal-Zellerfeld, Germany*

(Dated: December 16, 2015)

Alloying effects by $\text{T}=\text{Mn},\text{Co},\text{Ni}$ -substitution on FeS_2 have been investigated using density-functional calculations. The alloys $\text{Fe}_{1-x}\text{T}_x\text{S}_2$ have been investigated for concentrations $x = \frac{1}{4}, \frac{1}{2}, \frac{3}{4}$ together with the ground states of the pure compounds. The electronic structure is discussed with the goal to identify candidates for half metals, which are of interest for spintronics applications. We find interesting candidates at mean concentration of the Mn-doped FeS_2 and at low concentrations for Ni-doped materials. For the Mn alloys we also note the proximity to a low-spin to high spin transition. For Co-doped materials we reproduce the well known finding of half metallicity over the entire concentration range.

PACS numbers: 71.10.-w, 71.15.Nc, 71.15.Mb

I. INTRODUCTION

The rapid development in the emerging field of *spintronics*, or spin-electronics, has stimulated huge efforts to look for new materials utilized for creating new electronic devices^{1–6}. One of the key issues in this area is to obtain materials with high spin polarization at the Fermi level E_F , to be used as a source for polarized spin injection. The best candidates for this purpose are the so-called half-metallic ferromagnets (HMFs)^{1,7,8}. These HMFs are metallic for one spin direction and insulating for the opposite one, such offering a *complete*, i.e. 100 %, spin polarization of the charge carriers. However, it is first necessary to have a good understanding of the underlying behavior in these materials⁹. Many investigations have reported experimental evidence of either high or complete polarization in some oxides and compounds (CrO_2 ^{10,11}, Fe_3O_4 ^{11–13} and $\text{La}_{1-x}\text{Sr}_x\text{MnO}_3$ ^{14,15}).

Pyrite-type disulfides have attracted considerable interest for various reasons¹⁶. Semiconducting FeS_2 received widespread attention for its application in photovoltaic energy conversion^{17,18}. Substitution of Zn for Fe in iron pyrite has thus been used to tune the optical band gap in order to enhance the response to the solar spectrum¹⁹.

This class of materials has a variety of interesting properties²⁰. While FeS_2 is a van Vleck paramagnet, metallic CoS_2 displays long-range ferromagnetic order²¹.

In contrast, MnS_2 is found to be an antiferromagnetic insulator in the ground state, with a transition temperature of $T_N=48.2$ K.^{22–24} The insulating behavior is also found in NiS_2 , but with a disagreement about the ground state magnetic order. While some reports describe NiS_2 as an antiferromagnet^{25–27}, some others found it as a paramagnet^{28–30}. The insulating behavior of MnS_2 and NiS_2 has been attributed to the presence of strong electronic correlations^{31–38}. Some resonant photoemission studies³⁹, however, suggested that NiS_2 is a

p-to-*d* charge-transfer insulator rather than a *d*-*d* Mott-Hubbard insulator, with a gap between the occupied S *3p*-states and the empty Ni *3d*-states.

Among the pyrite-type disulfides, $\text{Fe}_{1-x}\text{Co}_x\text{S}_2$ has drawn much attention for spintronic applications. It is considered as a model for band gap tuning and for studying half-metallicity⁴⁰. It has been shown that the spin polarization in this system can be controlled with respect to alloying and should not be sensitive to crystallographic disorder⁴¹. Many experimental investigations and transport measurements have been carried out^{42–45}. Wang *et al*⁴³ have recently combined indirect transport probes with a direct measurement by PCAR (point contact Andréev reflection), to prove that the spin polarization can be continuously tuned over a wide range.

Moreover, several *ab-initio* calculations have been reported on the electronic structure of the $\text{Fe}_{1-x}\text{Co}_x\text{S}_2$ alloys^{41,46–48}. Zhao *et al*⁴⁶ predicted already in the early nineties on the basis of the Linear Combination of Atomic Orbital (LCAO) method that half-metallicity might be obtained when alloying FeS_2 with CoS_2 . A very important contribution has been the work by Mazin *et al*^{41,47} who performed detailed calculations using the Linear Muffin Tin Orbital (LMTO) method as well as the full-potential Linear Augmented Plane Wave (FP-LAPW) method. This work showed clearly that half-metallic ferromagnetism is present in the region $0.25 \leq x \leq 0.85$, with magnetic moments in a very good agreement with experiment.

Besides $\text{Fe}_{1-x}\text{Co}_x\text{S}_2$, some attempts⁴⁹ have been made to improve the band gap of FeS_2 . Different types of substitution have been tested ($\text{Fe}_{1-x}\text{T}_x\text{S}_2$, where $\text{T} = \text{Be}, \text{Mg}, \text{Ca}, \text{Os}, \text{Ru} \dots$ etc) in order to increase the gap for technical applications.

However, little attention has been paid to the $\text{Fe}_{1-x}(\text{Mn},\text{Ni})_x\text{S}_2$ systems, even-though the pure compounds (Mn and Ni disulfides) share the same pyrite crystal structure. In early experiments, $\text{Fe}_{1-x}\text{Ni}_x\text{S}_2$ solid solution has been synthesized^{31,50,51}.

Dilute substitution (less than 2%) of Fe in MnS_2 has been reported in experimental studies, using Mössbauer technique^{24,52}. Recently, Persson *et al.*⁵³ have investigated theoretically in the framework of GGA+U the spin transitions in $\text{Fe}_x\text{Mn}_{1-x}\text{S}_2$. It has been found that the spin transition pressure decreases with growing Fe substitution in MnS_2 .

In the present work, we investigate the $\text{Fe}_{1-x}(\text{Mn}, \text{Ni})_x\text{S}_2$ systems, in order to get a detailed picture of the ferromagnetic trends in the whole series, and to provide further insight into the mechanism of half-metallicity and spin polarization in these systems. The paper is organized as follows: In Sec. II, we describe the theoretical method and the computational details. A brief summary of the crystal structure is given in Sec III. In Sec. IV we present our results on the three compounds $\text{Fe}_{1-x}(\text{Mn}, \text{Co}, \text{Ni})_x\text{S}_2$. We summarize in Sec. V

II. COMPUTATIONAL METHOD

In the present study, we performed first-principles calculations in the framework of density-functional theory (DFT)^{54,55}. The exchange-correlation effects were taken into account within the generalized gradient approximation (GGA) of Perdew-Burke-Ernzerhof⁵⁶. We also performed some calculations using the PBE0r functional, which replaces a fraction of the exchange term of the PBE functional with the exact Fock-term^{57,58}. Unlike the PBE0⁵⁹ hybrid functional, we follow the idea of range separated hybrid functionals⁶⁰ and restrict this correction in the PBE0r functional to the onsite interactions in a local orbital basis.

The calculations have been performed with the Projector Augmented Wave (PAW) method⁶¹ as implemented in the CP-PAW code. The PAW method is an *all-electron* electronic structure method. The CP-PAW code is the original implementation of the PAW method and employs the framework of *ab-initio* molecular dynamics (AIMD)⁶² for the optimization of wave functions and atomic structure. For the augmentation, we used a $s^1p^1d^1$ set of projector functions for all atoms, where the superscripts denotes the number of projector functions angular momentum channel. A plane wave cutoff of 30 Ry has been chosen for the wave functions and 60 Ry for the charge density.

The Brillouin-zone integration has been performed with the linear tetrahedron method^{63,64} and the so-called Blöchl corrections⁶⁵. A $5 \times 5 \times 5$ k -point mesh has been used for the simple-cubic unit cell containing four transition-metal ions.

All structural parameters including the lattice parameters have been optimized.

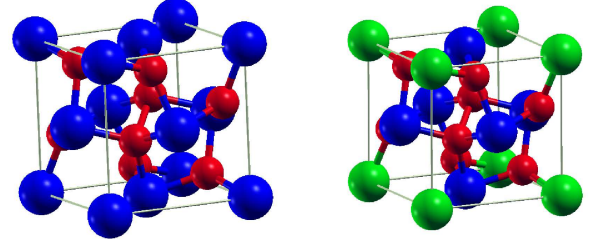


FIG. 1. (Color online) Crystal structures of the pure iron pyrite FeS_2 (left) and the substituted compound $\text{Fe}_{\frac{3}{4}}\text{Mn}_{\frac{1}{4}}\text{S}_2$ (right). Fe, Mn and S atoms are printed in blue, green and red, respectively.

III. CRYSTAL STRUCTURES

In this section, we describe the crystal structures used in our calculations. Many transition-metal disulfides TS_2 (with $\text{T} = \text{Mn}, \text{Fe}, \text{Co}, \text{Ni}, \text{Cu}, \text{Ru}$ and Os ... etc), crystallize in the cubic pyrite structure. The pyrite structure is based on a simple cubic (*sc*) lattice with space group $\text{Pa}\bar{3}(T_h^6)$ ^{17,66,67}. The transition-metal atoms occupy the Wyckoff positions (4a) and sulfur atoms occupy the positions (8c). The FeS_2 pyrite crystal structure is displayed in Fig.1, as well as an illustration of one alloyed compound $\text{Fe}_{\frac{3}{4}}\text{Mn}_{\frac{1}{4}}\text{S}_2$.

The pyrite crystal structure can be rationalized in terms of the *fcc*-NaCl structure with the sublattices occupied by transition-metal ions atoms and sulfur dimers, respectively. The sulfur dumbbells are oriented along the $\langle 111 \rangle$ axes. Because the distinct dumbbells are oriented in all four distinct $\langle 111 \rangle$ directions, the simple-cubic unit cell with four formula units of FeS_2 is employed.

Whereas the sulfur atoms are tetrahedrally coordinated by one sulfur and three iron atoms, the six nearest-neighbor sulfur atoms at each metal site form slightly distorted octahedra.

The pyrite structure is determined by the lattice constant and an internal parameter u . The internal parameter u and the lattice constant determine the bond length of the sulfur dumbbell as $d_{S-S} = \sqrt{3}(1-2u)a_{lat}$ and the Fe-S distance is $d_{Fe-S} = \sqrt{2}(1-u)^2 + u^2a_{lat}$.⁶⁸

The crystal structure of the pure disulfides is well established experimentally as well as theoretically (experimental data are included in table I). No structural information has been reported, however, for the alloyed compounds.

Calculated structural parameters and the lattice constants for the complete series are given in Table I. The bond lengths are averaged. Individual bond lengths differ by 0.2 %. from these averages. For the pure pure disulfides of Fe, Mn, Co, and Ni, the calculated bond lengths have been compared to experimental data³⁹ and found to deviate less than 0.5 %.

TABLE I. Calculated data lattice constants a (in Å), internal parameter u and averaged bond lengths of metal-sulfur and sulfur-sulfur bonds. Experimental data³⁹ are shown in parentheses.

$\text{Fe}_{1-x}\text{Mn}_x\text{S}_2$	$a[\text{\AA}]$	u	$d_{\text{Fe-S}}[\text{\AA}]$	$d_{\text{Mn-S}}[\text{\AA}]$	$d_{\text{S-S}}[\text{\AA}]$
$x = 0.00$	5.405 (5.416)	0.387 (0.385)	2.263		2.160
$x = 0.25$	5.432		2.257	2.272	2.274
$x = 0.50$	5.648		2.270	2.293	2.209
$x = 0.75$	5.832		2.411	2.432	2.411
$x = 1.00$	6.062(6.091)	0.402 (0.409)		2.527	2.620
$\text{Fe}_{1-x}\text{Co}_x\text{S}_2$				$d_{\text{Co-S}}$	
$x = 0.00$	5.405(5.416)	0.385 (0.385)	2.263		2.160
$x = 0.25$	5.420		2.249	2.285	2.181
$x = 0.50$	5.440		2.260	2.292	2.145
$x = 0.75$	5.471		2.264	2.296	2.125
$x = 1.00$	5.489 (5.539)	0.388 (0.390)	2.310		2.101
$\text{Fe}_{1-x}\text{Ni}_x\text{S}_2$				$d_{\text{Ni-S}}$	
$x = 0.00$	5.405 (5.416)	0.385 (0.385)	2.263		2.160
$x = 0.25$	5.445		2.247	2.340	2.146
$x = 0.50$	5.494		2.259	2.331	2.090
$x = 0.75$	5.542		2.249	2.325	2.042
$x = 1.00$	5.572 (5.620)	0.393 (0.394)	2.359		2.064

We considered those ordered alloy structures, that can be described within the simple cubic unit cell of pyrite. For each of the concentrations $x = \frac{1}{4}$, $x = \frac{1}{2}$, and $x = \frac{3}{4}$ only one symmetry inequivalent arrangement of the transition-metal sites exists. As seen in Fig.1 the minority alloying element for the occupations $x = \frac{1}{4}$ and $x = \frac{3}{4}$ occupies the cube corners, while the face centers are occupied with the majority element. For $x = \frac{1}{2}$, the alloying elements occupy alternating $\langle 001 \rangle$ planes.

IV. RESULTS AND DISCUSSIONS

The main goal of the present paper is the understanding of the effect of alloying FeS_2 with Mn, Co and Ni on the electronic and magnetic properties. In the following, we investigate the electronic properties of the three different alloys $\text{Fe}_{1-x}\text{Mn}(\text{Co}, \text{Ni})_x\text{S}_2$, and discuss the findings into the context of the pure compounds.

A. $\text{Fe}_{1-x}\text{Mn}_x\text{S}_2$

The density of states (DOS) of $\text{Fe}_{1-x}\text{Mn}_x\text{S}_2$ at $x = 0, \frac{1}{4}, \frac{1}{2}, \frac{3}{4}$ and 1 are shown in Fig.2.

The electronic structure of pure FeS_2 can be rationalized as follows: The sulfur dumbbells form negatively charged S_2^{2-} ions with all valence states filled except for the antibonding σ^* orbital between the sulfur ions. Consequently, each iron atom has an oxidation state 2+. The iron atom exists in a low-spin occupation with filled t_{2g} orbitals and empty e_g orbitals. Between the t_{2g} and the

e_g states exists a band gap of 0.69 eV in our calculations and ~ 0.9 eV in photoconductivity measurements^{18,30,69}. The underestimation is common for GGA calculations. It should be noted that the band gap in our calculations is determined by a conduction band state with sulfur character that extends with a very small density of states below the d-states.

The density of states of FeS_2 seen in the top graph of Fig. 2 is dominated by the sulfur p states forming a lower valence band extending from -8 eV to -2 eV. The sulfur s -states lie below the p -states and are outside the energy region shown. Above the sulfur states the $\text{Fe-}t_{2g}$ states form an isolated narrow band. Thus the valence-band edge is of $\text{Fe-}t_{2g}$ character. The conduction band is actually a tail of predominantly sulfur character, which extends below the prominent $\text{Fe-}e_g$ states, which rise up at about +1 eV. Due to the small density of states the tail of the sulfur states is easily overlooked and it is hardly visible in the figure.

At first, we investigated the concentration dependence on the basis of ferromagnetically aligned Mn-ions. This is the case of technological interest, because the spins may be aligned by an external magnetic field. The corresponding results are shown in Fig. 2. The relative stability of the ferromagnetic order relative to antiferromagnetic states will be addressed later in this section.

The Mn- t_{2g} states are located in the same energy region as the $\text{Fe-}t_{2g}$ states. Because the Mn ions have one electron less than the Fe ions, the Mn- t_{2g} states have a hole in the t_{2g} shell. This spin of this hole results in a magnetic moment, so that the majority-spin and minority-spin states of Mn- t_{2g} character are shifted

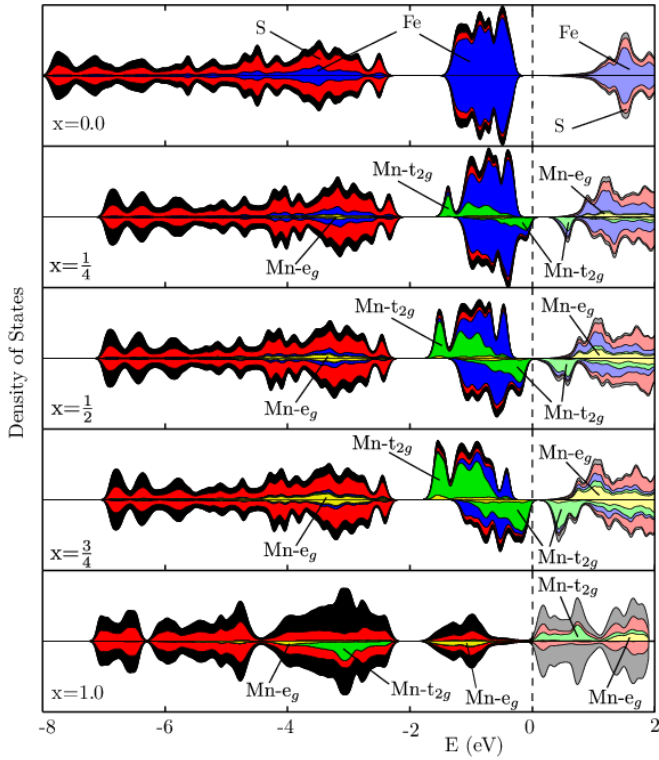


FIG. 2. (Color online) Density of states (DoS) of $\text{Fe}_{1-x}\text{Mn}_x\text{S}_2$ alloys for $x = 0, \frac{1}{4}, \frac{1}{2}, \frac{3}{4}$ and for $x = 1$. The origin of the energy axis is set to the Fermi level E_F , which is indicated by the dashed line. The DoS of spin-down electrons is drawn with the axis pointing downward. The total density of states is given by the black envelope. The projected DoS are drawn as distinct colored areas on top of the total DoS. The DoS of the Fe-d states are represented by the blue area and the DoS of the sulfur states by the red area. The dopant (Mn) $3d$ states are divided into t_{2g} states shown in green and e_g states shown in yellow. For the antiferromagnetic MnS_2 the projected DoS of the d-states is shown only for those Mn with the majority-spin direction in the down channel.

against each other. The top of the valence band in the majority-spin direction is of Fe character while that of the minority-spin direction is of Mn character.

Substitutional alloying Mn for Fe introduces empty states into the gap between t_{2g} and e_g states of FeS_2 . These states derive from a Mn- t_{2g} orbitals. The Mn ions exist in a low-spin 2+ oxidation state, for which the e_g orbitals are empty and the t_{2g} are filled except for one orbital, which appears in the band gap.

The majority-spin direction has a band gap with only a weak concentration dependence. This gap decreases abruptly from 0.69 eV in FeS_2 to 0.37-0.41 eV in the alloys. In contrast, the band gap in the minority-spin direction shrinks with increasing concentration as the empty t_{2g} states hybridize more effectively.

For low concentration, i.e. for $x = 0.25$, a semiconductor is obtained with a band gap of 0.35 eV. Valence and conduction band are both in the minority-spin direction. The electron transport properties are thus dominated by

a single spin direction.

At larger Mn concentration, that is for $x = \frac{1}{2}$ and $x = \frac{3}{4}$, the minority-spin band gap almost collapses with E_g below 0.01 eV. Because this band gap is in the minority-spin direction, this material can be considered a half metal for practical purposes. We expect this material to be of interest for spintronics applications.

The Fermi-level moves, however, at higher concentration close to the conduction-band bottom of the majority-spin direction. This is not immediately evident from Fig. 2 because of the low density of states in the conduction band of the majority-spin direction.

After having discussed the electronic structure of the alloys in the ferromagnetic state, we investigated their stability relative to a competing antiferromagnetic phase. We investigated the type-III single-k antiferromagnetic ordering, which has been established experimentally³⁶ for MnS_2 , as well as the order with antiferromagnetically coupled (111) planes. The former requires to double the unit cell in $\langle 100 \rangle$ direction.

Both antiferromagnetic arrangements produce analogous results: The ferromagnetic order is stable for low Mn concentration, $x = \frac{1}{4}$ and $x = \frac{1}{2}$, while at higher Mn concentration $x = \frac{3}{4}$ and $x = 1$ the antiferromagnetic order is favorable.

The antiferromagnetic materials are described as metals. The metallic behavior of the antiferromagnets is attributed to a deficiency of the density functionals used. Calculations with hybrid functionals produce an insulating ground state.

Thus, our calculations predict half-metallic behavior in the half-doped regime. At lower concentration the material becomes more insulating, while at higher doping, that is between $x = \frac{1}{2}$ and $x = \frac{3}{4}$, the material turns antiferromagnetic. It may be possible to stabilize the ferromagnetic order also for higher concentrations through an external magnetic field.

The low-spin character of the Mn-ions in the alloys differs from the high-spin character of the pure MnS_2 . Even in the GGA calculations, that is without the Fock term, we find the pure compound to be a high-spin antiferromagnet, in agreement with recent GGA calculations⁵³. Experimentally, MnS_2 is found to be an antiferromagnetic insulator³⁶. The calculated band gap within GGA vanishes, while the local hybrid functionals with an admixture of 10 % of Fock exchange provides a band gap of 0.91 eV in agreement with experiment of 1 eV⁷⁰.

Performing calculations with a local hybrid functional for the alloys, we noticed that the the system is close to a transition between low-spin and to high-spin Mn states. Replacing more than 5% of the PBE exchange by the local Fock term drives the Mn ions into a high-spin state with a filled d-shell in the majority-spin direction and an empty d-shell in the minority-spin direction. In this configuration that compound is an insulator. Using hybrid calculations with a Fock-exchange admixture of 10%, we obtain the high-spin configuration of Mn ions for all concentrations considered.

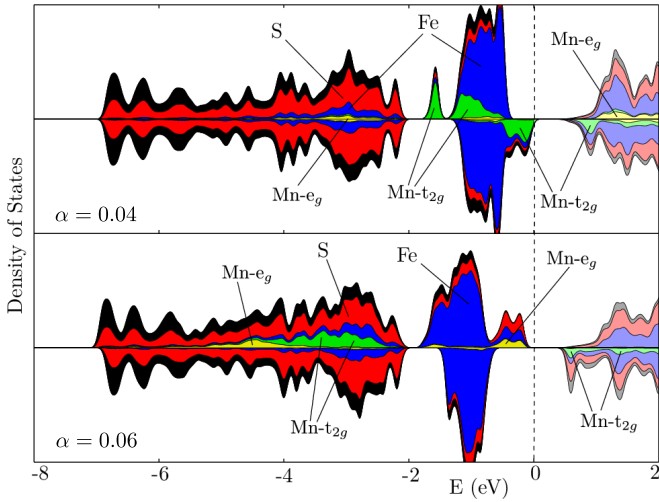


FIG. 3. (Color online) Density of states (DoS) of $\text{Fe}_{\frac{3}{4}}\text{Mn}_{\frac{1}{4}}\text{S}_2$ alloy, in the low spin (upper panel) and high spin (lower panel) states of Mn, using hybrid functionals. Two different weights of the Fock term, ($\alpha=0.04$ and $\alpha=0.06$), have been used to direct the system into the respective configuration. Further description as in Fig. 2.

Similar results have been obtained by Persson *et al*⁵³ using the GGA+U method within the implementation of Liechtenstein *et al*⁷¹. They have shown the existence of high-spin to low-spin transitions for $x = \frac{1}{4}$, $x = \frac{1}{2}$ and $x = \frac{3}{4}$, and they calculated the corresponding pressure of transition.

To illustrate this transition between low-spin and to high-spin, we show in Fig. 3 the density of states for low-spin and high-spin for $x = \frac{1}{4}$. We used hybrid functionals with two Fock term weights, namely $\alpha = 0.04$ and $\alpha = 0.06$, to show the main changes due to the transition. The different values have been chosen to guide the system into the chosen configuration.

In the low-spin configurations that Mn-t_{2g} states are filled except for one hole in the minority-spin direction. The e_g states on the other hand are empty. In the high-spin configuration, all majority-spin d-states on Mn are occupied and all minority spin d-states are empty.

B. $\text{Fe}_{1-x}\text{Co}_x\text{S}_2$

Let us now turn to the alloy $\text{Fe}_{1-x}\text{Co}_x\text{S}_2$. It has been studied in detail, both experimentally^{43,48} and theoretically^{41,47}, and our results are consistent with previous ones. They are added here for the sake of consistency and completeness.

The density of states of the series with $x = 0, \frac{1}{4}, \frac{1}{2}, \frac{3}{4}$ and 1 is given in Fig. 4. It agrees with DFT calculations by Umemoto *et al*⁴⁷. The calculated electronic structure agrees also well with other theoretical and experimental data found in literature^{43,48}.

The Co²⁺ ions have a filled t_{2g} shell and one electron

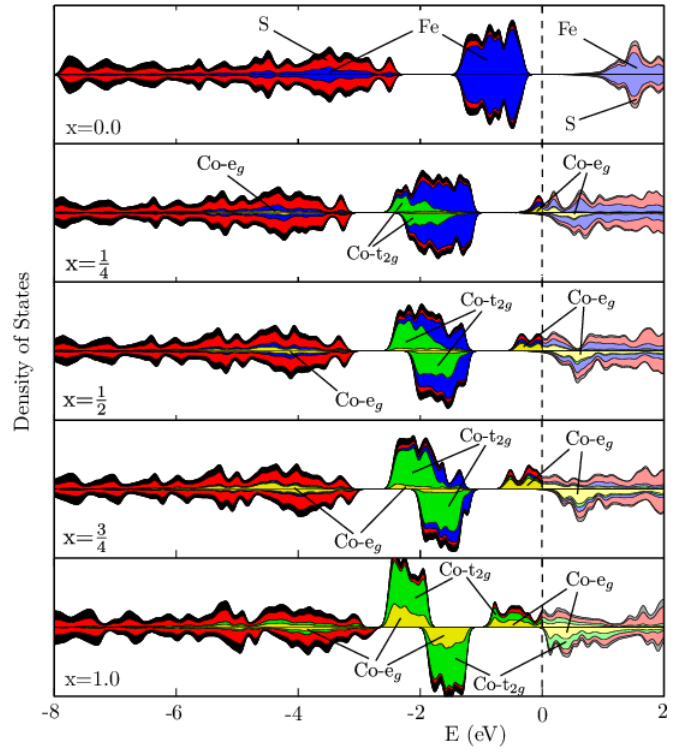


FIG. 4. (Color online) Density of states (DoS) of $\text{Fe}_{1-x}\text{Co}_x\text{S}_2$ alloys for $x = 0, \frac{1}{4}, \frac{1}{2}, \frac{3}{4}$ and for $x = 1$. Further description as in Fig. 2.

in the e_g shell. The Fermi level is pinned in the e_g states of Co of the majority-spin direction. As a consequence the alloys with Co are half metals.

The Co-t_{2g} states are located in the same energy region as the Fe-t_{2g} states, i.e. in the upper part of the valence band between -3 eV and -1 eV, for all the alloys. The Co-e_g bands form the lower part of the conduction band. However, some weight is also present in the top region of the occupied sulfur p-band between -5.5 eV and -3.5 eV. The spin splitting of the Co-t_{2g} states is smaller than that of the Mn-ions in the $\text{Fe}_{1-x}\text{Mn}_x\text{S}_2$ alloys.

C. $\text{Fe}_{1-x}\text{Ni}_x\text{S}_2$

Early experimental studies⁵¹ investigated the $\text{Fe}_{1-x}\text{Ni}_x\text{S}_2$ alloys for concentrations $0.4 \leq x \leq 0.6$. In this range of substitution, their magnetic measurements have shown that $\text{Fe}_{1-x}\text{Ni}_x\text{S}_2$ are paramagnetic metals.

The alloying effect of FeS₂ with Ni can be understood again from the the point of view of Ni²⁺ ions. Ni²⁺ has a half-filled e_g shell being occupied with two electrons. The near degeneracy of e_g states is lifted by Hund's rule splitting, which concentrates both e_g electrons in one spin direction which results in magnetic ions.

For low concentration, i.e. for $x = \frac{1}{4}$, we find a conduction band in the minority-spin direction of predominantly Ni-e_g character. It is separated by a band gap of

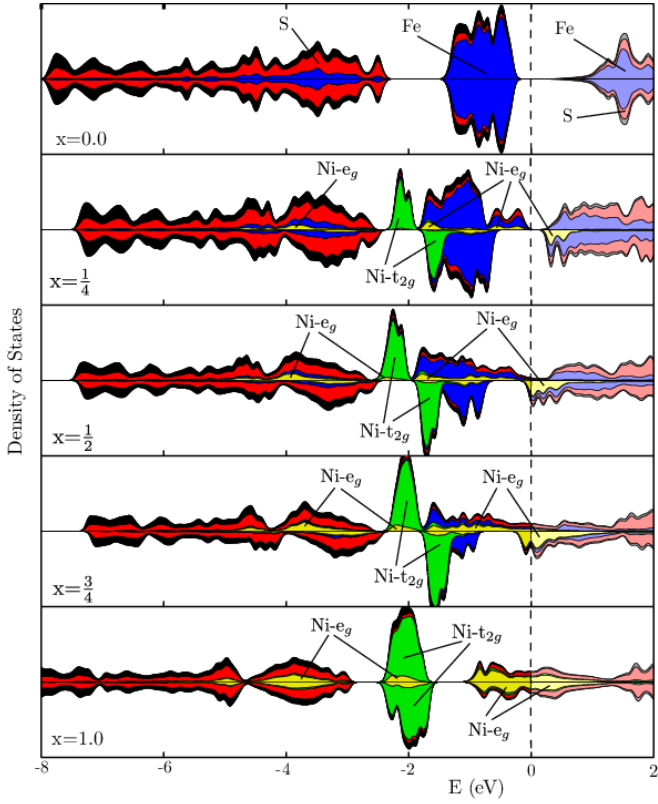


FIG. 5. (Color online) Density of states (DoS) of $\text{Fe}_{1-x}\text{Ni}_x\text{S}_2$ alloys for $x = 0, \frac{1}{4}, \frac{1}{2}, \frac{3}{4}$ and for $x = 1$. The origin of the energy axis is set to E_F , which is indicated by the dashed line. The total density of states is given by the black envelope. The projected density of states are drawn as distinct colored areas on top of the total density of states. The Fe DoS are represented by the blue area and the sulfur DoS by the red area. The Ni-3d states are divided into t_{2g} states shown in yellow and e_g states shown in green

0.77 eV from the Fe- t_{2g} states. In the majority-spin direction, we find filled Ni e_g states below the Fermi level that are strongly hybridized with sulfur and Fe- t_{2g} states. In the majority-spin direction valence and conduction bands overlap, which turns this material into a half-metal.

At higher concentration, i.e. for $x = \frac{1}{2}, \frac{3}{4}$, the Fermi level shifts into the formerly empty Ni- e_g band of the minority spin direction. These electrons are removed from the states that derive from the majority-spin Ni- e_g states.

As a consequence, the magnetic moment decreases with increasing concentration from $2 \mu_B$ per Ni atom for $x = 0$ to $1.7 \mu_B$ per Ni atom for $x = \frac{1}{2}$ and to $1.3 \mu_B$ per Ni atom for $x = \frac{3}{4}$.

In agreement with the experimental magnetic ordering²⁷, pure NiS_2 is found to be an antiferromagnet. However, the obtained metallic character disagrees with experiments²⁸, which find a semiconducting ground state

with an indirect band gap of 0.27 eV. This metallic behavior is attributed to the well-known band gap problem of DFT. To resolve this issue, we carried out local hybrid functional calculations and found an NiS_2 semiconductor with a gap of ~ 0.4 eV consistent with experiment.

In view of the magnetic results of NiS_2 , we explored the stability of the $\text{Fe}_{1-x}\text{Ni}_x\text{S}_2$ alloys against a transition to an antiferromagnetic order. We explored the stability of the same two antiferromagnetic orders used before for the Mn-Fe alloys. In contrast to the Mn-Fe system, however, the Ni-Fe alloys remain ferromagnetic for all alloys studied $x = \frac{1}{4}, \frac{1}{2}$ and $\frac{3}{4}$.

Comparing the alloys with Mn, Co, and Ni, we observe the trend that the d-bands shift down in energy with increasing atomic number due to the Coulomb attraction to the increased nuclear charge.

V. SUMMARY AND CONCLUSION

Using first-principles calculations, we explored the possibility of obtaining half metals by alloying the transition metals Mn, Co, and Ni to FeS_2 . Alloys with dopant concentration $x = \frac{1}{4}, \frac{1}{2}$ and $x = \frac{3}{4}$ have been investigated together with the pure compounds. Having the application on spintronics in mind, this work focusses on the ferromagnetic states. For the $\text{Fe}_{1-x}\text{Co}_x\text{S}_2$ alloys, we confirm previous experimental and theoretical results. We provide indications which alloys are promising candidates for half metals.

For the Mn doped alloys, we obtain a semiconductor at low concentration. At higher concentrations this gap closes in the minority-spin direction for all practical purposes. Thus we expect this material to be suitable as a half-metal. It should be noted, however, that the material is close to a low-spin to high-spin transition, which can be triggered by changing the density functional to hybrid functionals. In the high-spin configuration we obtain the material to be insulating.

For the $\text{Fe}_{1-x}\text{Co}_x\text{S}_2$ alloy, half-metallic ferromagnets are obtained for the full range of concentrations investigated. The system

For the Ni-doped alloys we obtain a half metal for low doping, i.e. for $x = \frac{1}{4}$. At higher doping the system turns into a full metal.

ACKNOWLEDGMENTS

A.H. gratefully acknowledges financial support by Bejaia university. Financial support by the Deutsche Forschungsgemeinschaft through FOR 1346 is gratefully acknowledged.

* corresponding author: abdeslam.houari@univ-bejaia.dz

¹ M. Bowen, M. Bibes, A. Barthlmy, J.-P. Con-

tour, A. Anane, Y. Lemaître, and A. Fert, *Applied Physics Letters* **82**, 233 (2003).

² S. A. Wolf, D. D. Awschalom, R. A. Buhrman, J. M. Daughton, S. von Molnr, M. L. Roukes, A. Y. Chtchelkina, and D. M. Treger, *Science* **294**, 1488 (2001).

³ J. Kortright, D. Awschalom, J. Sthr, S. Bader, Y. Idzlerda, S. Parkin, I. K. Schuller, and H.-C. Siegmann, *Journal of Magnetism and Magnetic Materials* **207**, 7 (1999).

⁴ G. Gryniewich, J. kerman, P. Brown, B. Butcher, R. Dave, M. DeHerrera, M. Durlam, B. Engel, J. Janesky, S. Pietambaram, N. Rizzo, J. Slaughter, K. Smith, J. Sun, and S. Tehrani, *MRS Bulletin* **29**, 818 (2004).

⁵ A. Houari, S. F. Matar, M. A. Belkhir, and M. Nakhl, *Phys. Rev. B* **75**, 064420 (2007).

⁶ A. Houari, S. Matar, and M. Belkhir, *Computational Materials Science* **43**, 392 (2008).

⁷ C. M. Fang, G. A. de Wijs, and R. A. de Groot, *Journal of Applied Physics* **91**, 8340 (2002).

⁸ A. Houari, S. F. Matar, and V. Eyert, *Phys. Rev. B* **82**, 241201 (2010).

⁹ J. E. Pask, L. H. Yang, C. Y. Fong, W. E. Pickett, and S. Dag, *Phys. Rev. B* **67**, 224420 (2003).

¹⁰ K. P. Kämper, W. Schmitt, G. Güntherodt, R. J. Gambino, and R. Ruf, *Phys. Rev. Lett.* **59**, 2788 (1987).

¹¹ J. S. Parker, P. G. Ivanov, D. M. Lind, P. Xiong, and Y. Xin, *Phys. Rev. B* **69**, 220413 (2004).

¹² Y. S. Dedkov, U. Rüdiger, and G. Güntherodt, *Phys. Rev. B* **65**, 064417 (2002).

¹³ S. Morton, G. Waddill, S. Kim, I. K. Schuller, S. Chambers, and J. Tobin, *Surface Science* **513**, L451 (2002).

¹⁴ J.-H. Park, E. Vescovo, H.-J. Kim, C. Kwon, R. Ramesh, and T. Venkatesan, *Phys. Rev. Lett.* **81**, 1953 (1998).

¹⁵ B. Nadgorny, I. I. Mazin, M. Osofsky, R. J. Soulén, P. Broussard, R. M. Stroud, D. J. Singh, V. G. Harris, A. Arsenov, and Y. Mukovskii, *Phys. Rev. B* **63**, 184433 (2001).

¹⁶ J. B. Goodenough, *Journal of Solid State Chemistry* **3**, 26

¹⁷ V. Eyert, K.-H. Höck, S. Fiechter, and H. Tributsch, *Phys. Rev. B* **57**, 6350 (1998).

¹⁸ A. Ennaoui, S. Fiechter, C. Pettenkofer, N. Alonso-Vante, K. Bker, M. Bronold, C. Hpfner, and H. Tributsch, *Solar Energy Materials and Solar Cells* **29**, 289 (1993).

¹⁹ K. Büker, S. Fiechter, V. Eyert, and H. Tributsch, *Journal of The Electrochemical Society* **146**, 261 (1999), <http://jes.ecsdl.org/content/146/1/261.full.pdf+html>.

²⁰ W. Temmerman, P. J. Durham, and D. Vaughan, *Phys. Chem. Minerals* **20**, 249 (1993).

²¹ D. Hobbs and J. Hafner, *Journal of Physics: Condensed Matter* **11**, 8197 (1999).

²² J. Hastings and L. Corliss, *Physical Review B* **14**, 1995 (1976).

²³ T. Chattopadhyay, T. Brückel, and P. Burlet, *Solid. State. Comm* **50**, 865 (1984).

²⁴ M. A. S. Khan, V. H. McCann, J. B. Ward, and R. J. Pollard, *Journal of Physics C: Solid State Physics* **16**, 4011 (1983).

²⁵ G. Krill, M. F. Lapierre, C. Robert, F. Gautier, G. Czjzek, J. Fink, and H. Schmidt, *Journal of Physics C: Solid State Physics* **9**, 761 (1976).

²⁶ A. Y. Matsuura, Z. X. Shen, D. S. Dessau, C. H. Park, T. Thio, J. W. Bennett, and O. Jepsen, *Phys. Rev. B* **53**, R7584 (1996).

²⁷ X. Yao, J. M. Honig, T. Hogan, C. Kannewurf, and J. Spalek, *Phys. Rev. B* **54**, 17469 (1996).

²⁸ R. L. Kautz, M. S. Dresselhaus, D. Adler, and A. Linz, *Phys. Rev. B* **6**, 2078 (1972).

²⁹ K. Kikuchi, T. Miyadai, T. Fukui, H. It, and K. Takizawa, *Journal of the Physical Society of Japan* **44**, 410 (1978), <http://dx.doi.org/10.1143/JPSJ.44.410>.

³⁰ E. K. Li, K. H. Johnson, D. E. Eastman, and J. L. Freeouf, *Phys. Rev. Lett.* **32**, 470 (1974).

³¹ T. A. Bither, R. J. Bouchard, W. H. Cloud, P. C. Donohue, and W. J. Siemons, *Inorganic Chemistry* **7**, 2208 (1968).

³² K. Adachi, K. Sato, K. Yamauchi, and M. Ohashi, *Journal of the Physical Society of Japan* **32**, 573 (1972).

³³ S. Ogawa, *Journal of Applied Physics* **50**, 2308 (1979).

³⁴ J. Hastings and L. Corliss, *IBM Journal of Research and Development* **14**, 227 (1970).

³⁵ T. Miyadai, K. Kikuchi, and Y. Ito, *Physica B+C* **8688**, Part 2, 901 (1977).

³⁶ T. Chattopadhyay, T. Brückel, and P. Burlet, *Phys. Rev. B* **44**, 7394 (1991).

³⁷ A. E. Bocquet, K. Mamiya, T. Mizokawa, A. Fujimori, T. Miyadai, H. Takahashi, M. Mri, and S. Suga, *Journal of Physics: Condensed Matter* **8**, 2389 (1996).

³⁸ H. Hiraka, Y. Endoh, and K. Yamada, *Journal of Magnetism and Magnetic Materials* **177181**, Part 2, 1349 international Conference on Magnetism (Part II).

³⁹ A. Fujimori, K. Mamiya, T. Mizokawa, T. Miyadai, T. Sekiguchi, H. Takahashi, N. Môri, and S. Suga, *Phys. Rev. B* **54**, 16329 (1996).

⁴⁰ L. Wang, T. Y. Chen, and C. Leighton, *Phys. Rev. B* **69**, 094412 (2004).

⁴¹ I. I. Mazin, *Applied Physics Letters* **77**, 3000 (2000).

⁴² K. Ramesha, R. Seshadri, C. Ederer, T. He, and M. A. Subramanian, *Phys. Rev. B* **70**, 214409 (2004).

⁴³ L. Wang, K. Umemoto, R. M. Wentzcovitch, T. Y. Chen, C. L. Chien, J. G. Checkelsky, J. C. Eckert, E. D. Dahlberg, and C. Leighton, *Phys. Rev. Lett.* **94**, 056602 (2005).

⁴⁴ L. Wang, T. Y. Chen, C. L. Chien, and C. Leighton, *(1971)Applied Physics Letters* **88**, 232509 (2006).

⁴⁵ S. F. Cheng, G. T. Woods, K. Bussmann, I. I. Mazin, R. J. Soulén, E. E. Carpenter, B. N. Das, and P. Lubitz, *Journal of Applied Physics* **93**, 6847 (2003).

⁴⁶ G. L. Zhao, J. Callaway, and M. Hayashibara, *Phys. Rev. B* **48**, 15781 (1993).

⁴⁷ K. Umemoto, R. M. Wentzcovitch, L. Wang, and C. Leighton, *physica status solidi (b)* **243**, 2117 (2006).

⁴⁸ C. Leighton, M. Manno, A. Cady, J. W. Freeland, L. Wang, K. Umemoto, R. M. Wentzcovitch, T. Y. Chen, C. L. Chien, P. L. Kuhns, M. J. R. Hoch, A. P. Reyes, W. G. Moulton, E. D. Dahlberg, J. Checkelsky, and J. Eckert, *Journal of Physics: Condensed Matter* **19**, 315219 (2007).

⁴⁹ R. Sun and G. Ceder, *Phys. Rev. B* **84**, 245211 (2011).

⁵⁰ R. Bouchard, *Materials Research Bulletin* **3**, 563 (1968).

⁵¹ T. Bither, P. Donohue, W. Cloud, P. Bierstedt, and H. Young, *Journal of Solid State Chemistry* **1**, 526 (1970).

⁵² C. B. Bergeron, M. Avinor, and H. Drickamer, *Inorganic Chemistry* **10**, 1338 (1971).

⁵³ K. Persson, G. Ceder, and D. Morgan, *Phys. Rev. B* **73**, 115201 (2006).

⁵⁴ P. Hohenberg and W. Kohn, *Phys. Rev.* **136**, B864 (1964).

⁵⁵ W. Kohn and L. J. Sham, *Phys. Rev.* **140**, A1133 (1965).

⁵⁶ J. P. Perdew, K. Burke, and M. Ernzerhof, *Phys. Rev. Lett.* **77**, 3865 (1996).

⁵⁷ A. D. Becke, *J. Chem. Phys.* **98**, 1372 (1993).

⁵⁸ J. P. Perdew, M. Ernzerhof, and K. Burke, *J. Chem. Phys.*

105, 9982 (1996).
⁵⁹ C. Adamo and V. Barone, *J. Chem. Phys.* **110**, 6158 (1999).
⁶⁰ J. Heyd, G. Scuseria, and M. Ernzerhof, *J. Chem. Phys.* **118**, 8207 (2003).
⁶¹ P. E. Blöchl, *Phys. Rev. B* **50**, 17953 (1994).
⁶² R. Car and M. Parrinello, *Phys. Rev. Lett.* **55**, 2471 (1985).
⁶³ O. Jepsen and O. Andersen, *Sol. St. Commun.* **9**, 1763 (1971).
⁶⁴ G. Lehmann and M. Taut, *Phys. Stat. Sol. B* **54**, 469 (1972).
⁶⁵ P. E. Blöchl, O. Jepsen, and O. K. Andersen, *Phys. Rev. B* **49**, 16223 (1994).
⁶⁶ S. L. Finklea, III, L. Cathey, and E. L. Amma, *Acta Crystallographica Section A* **32**, 529 (1976).
⁶⁷ E. D. Stevens, M. L. DeLucia, and P. Coppens, *Inorganic Chemistry* **19**, 813 (1980).
⁶⁸ M. Birkholz and R. Rudert, *Phys. Stat. Sol. B* **245**, 1858 (2008).
⁶⁹ A. Schlegel and P. Wachter, *Journal of Physics C: Solid State Physics* **9**, 3363 (1976).
⁷⁰ G. Brostigen, *Acta Chemica Scandinavica* **24**, 2993 (1970).
⁷¹ A. I. Liechtenstein, V. I. Anisimov, and J. Zaanen, *Phys. Rev. B* **52**, R5467 (1995).